

Cosmological implications of Standard Model criticality and Higgs inflation

Yuta Hamada,^{*1,2} Hikaru Kawai,^{†3} Yukari Nakanishi,^{‡4} and Kin-ya Oda^{§4}

¹*Department of Physics, University of Wisconsin, Madison, WI 53706, USA*

²*KEK Theory Center, IPNS, KEK, Tsukuba, Ibaraki 305-0801, Japan*

³*Department of Physics, Kyoto University, Kyoto 606-8502, Japan*

⁴*Department of Physics, Osaka University, Osaka 560-0043, Japan*

January 25, 2021

Abstract

The observed Higgs mass indicates that the Standard Model can be valid up to near the Planck scale M_{P} . Within this framework, it is important to examine how little modification is necessary to fit the recent experimental results in particle physics and cosmology. As a minimal extension, we consider the possibility that the Higgs field plays the role of inflaton and that the dark matter is the Higgs-portal scalar field. We assume that the extended Standard Model is valid up to the string scale 10^{17} GeV. (This translates to the assumption that all the non-minimal couplings are not particularly large, $\xi \lesssim 10^2$, as in the critical Higgs inflation, since $M_{\text{P}}/\sqrt{10^2} \sim 10^{17}$ GeV.) We find a correlated theoretical bound on the tensor-to-scalar ratio r and the dark matter mass m_{DM} . As a result, the Planck bound $r < 0.09$ implies that the dark-matter mass must be smaller than 1.1 TeV, while the PandaX-II bound on the dark-matter mass $m_{\text{DM}} > 0.7 \pm 0.2$ TeV leads to $r \gtrsim 2 \times 10^{-3}$. Both are within the range of near-future detection. When we include the right-handed neutrinos of mass $M_{\text{R}} \sim 10^{14}$ GeV, the allowed region becomes wider, but we still predict $r \gtrsim 10^{-3}$ in the most of the parameter space. The most conservative bound becomes $r > 10^{-5}$ if we allow three-parameter tuning of m_{DM} , M_{R} , and the top-quark mass.

*yhamada@wisc.edu

†hkawai@gauge.scphys.kyoto-u.ac.jp

‡nakanishi@het.phys.sci.osaka-u.ac.jp

§odakin@phys.sci.osaka-u.ac.jp

Contents

1	Introduction	3
2	Lower bound on tensor-to-scalar ratio	4
3	Z_2 Higgs-portal scalar model	6
4	Analysis without heavy right-handed neutrinos	8
4.1	Method of analysis	8
4.2	Results	8
5	Analysis with right-handed neutrinos	10
5.1	Method of analysis	10
5.2	Results for Normal Hierarchy	11
5.3	Results for Inverted Hierarchy	13
5.4	Results for Degenerate case	15
6	Allowed region for all parameter space	16
6.1	Lower bound on r for each M_R	16
6.2	Lower bound on r for each m_t	17
7	Summary and discussion	21
A	Renormalization group equations	22
B	Explaining the form of envelope by potential shape	24

1 Introduction

The Higgs field is the only elementary scalar whose existence is experimentally confirmed.¹ The observed Higgs mass indicates that the Standard Model (SM) can be valid up to near the Planck scale $M_{\text{P}} = 1/\sqrt{8\pi G} \simeq 2.4 \times 10^{18}$ GeV, that is, all the couplings remain perturbative and the Higgs potential is stable; see e.g. Refs. [3, 4, 5, 6, 7, 8, 9, 10, 11, 12, 13, 14, 15, 16].² From string-theory point of view, this fact suggests that string theory is directly connected to the SM at the string scale $\Lambda \sim 10^{17}$ GeV.

Furthermore, the Higgs potential can be very small and flat around the Planck scale by tuning the top quark mass within the experimental error. This fact, the so-called criticality of the SM, suggests that something non-trivial is happening around the Planck scale and that the SM remains valid without much modification up to the scale.³ Within this paradigm, it is important to examine how little modification is necessary to fit the recent experimental results in particle physics and cosmology, especially the inflation and the dark matter.

The flatness of the Higgs potential suggests that the Higgs field can play the role of inflaton. Indeed, if we trust the SM even at the Planck scale, we can realize a phenomenologically viable inflation, namely the critical Higgs inflation, by introducing a non-minimal coupling of order $10\text{--}10^2$ [56, 57, 58]; see also Ref. [59].⁴

In this paper, we *do not assume any particular form* of the Higgs potential at the Planck scale.⁵ Instead, we study consequences of a general postulate that the Higgs field plays the role of inflaton above the string scale, assuming that the SM (extended with dark matter) is reliable below it; see Fig. 1.⁶ After the end of the inflation, the slow-roll condition on the Higgs field is violated. In order for the fields to roll down to the electroweak (EW) scale, the potential height must be smaller than the inflation energy V_{inf} in the whole region $\varphi \leq \Lambda$. Note that even if there exists a local maximum with its height smaller than V_{inf} , it does not interrupt the rolling down to the EW scale because the slow-roll condition is already violated. As we do not specify the shape of the inflaton potential above Λ , we cannot predict precisely the cosmological parameters such as the spectral index n_s and the tensor-to-scalar ratio r . However, we may still put a lower bound on V_{inf} from the highest value of the Higgs potential in the region $\varphi < \Lambda$, which can be converted into the lower bound on r .

It is certain that there exists a dark matter (DM). As one of the simplest realization, we employ the Higgs portal Z_2 scalar dark matter model [64, 65, 66, 67, 68, 69, 70, 71, 72],⁷ though our analysis itself is applicable for any other model that modifies the running of the

¹There always remains a possibility that the Higgs field turns out to be a composite field in an unexplored energy region; see e.g. Refs. [1, 2] for recent reviews.

²See Refs. [17, 18, 19, 20, 7] for the renormalization group analyses on the vacuum stability including the right-handed neutrinos.

³This paradigm includes e.g. the multiple point criticality principle (MPP) [21, 22, 23, 24, 25], the (classical) conformality [26, 27, 26, 28, 29, 30, 31, 32, 33, 34, 35, 36, 37, 38, 39, 40, 41, 42, 43, 44, 45], the asymptotic safety [46, 47, 48], the hidden duality and symmetry [49, 50], and the maximum entropy principle [51, 52, 53, 54, 55].

⁴In the original Higgs inflation model [60, 61], the flatness of the Higgs potential has not been assumed and a large non-minimal coupling $\xi \sim 10^{4-5}$ has been required.

⁵If one assumes e.g. that the Higgs field fits in the massless state in string theory, one may compute the potential at the trans-Planckian scale and discuss the possibility of its mixing with other directions such as the radius of the extra dimension at the high scales [62, 63].

⁶This is consistent with the natural assumption that all the non-minimal couplings are not particularly large, namely, at most 10^2 , as in the critical Higgs inflation.

⁷See Ref. [73] for a model with extra dark Higgs field.

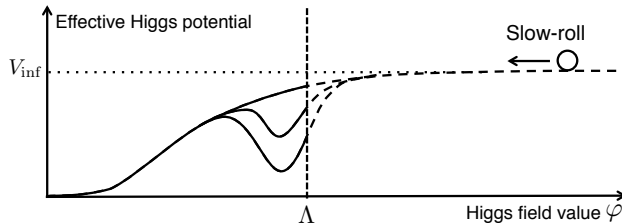


Figure 1: Schematic figure for the Higgs field as an inflaton

Higgs quartic coupling. We consider the generic region of the DM mass m_{DM} being larger than the Higgs mass. Then its thermal abundance fixes the relation between the DM mass and the Higgs-DM coupling κ to be $m_{\text{DM}} \simeq \kappa \times 3.2 \text{ TeV}$, and the spin-independent DM-nucleon elastic cross section is determined to be $\sigma_{\text{SI}} \sim 10^{-45} \text{ cm}^2$ [74, 75]; see Fig. 2 for more discussion. The latest 1.6σ bound from the PandaX-II experiment [76] reads $m_{\text{DM}} \gtrsim 0.7 \text{ TeV}$. When we do not include the right-handed neutrinos, we find that the current observational bounds $r < 0.09$ and $m_{\text{DM}} \gtrsim 0.7 \text{ TeV}$ lead to the theoretical bounds $m_{\text{DM}} \lesssim 1.1 \text{ TeV}$ and $r \gtrsim 2 \times 10^{-3}$, respectively, which are well within the range of near future detection.

We have also studied the case with the right-handed neutrinos that account for the observed neutrino oscillations through the seesaw mechanism [77, 78]. We find that when their mass is in the range $M_{\text{R}} \lesssim 10^{13} \text{ GeV}$, the results are the same as in the case without them. As we increase M_{R} , the bound becomes milder up to the scale 10^{14} GeV , and then becomes tighter up to 10^{15} GeV at which the right-handed neutrino contribution makes the Higgs potential unstable. Combining these results, we find the absolute theoretical bound $r > 10^{-5}$. If we restrict $m_{\text{DM}} \gtrsim 1.3 \text{ TeV}$, we obtain a stronger bound $r \gtrsim 10^{-3}$ for a reasonable top-quark mass range, as we will see in Fig. 7.

This paper is organized as follows. In Sec. 2, we show our basic strategy how to put a lower bound on r without the knowledge of higher scales. In Sec. 3, we review the Higgs-portal Z_2 scalar dark matter. In Sec. 4, we show our results without the effects from the heavy right-handed neutrinos. In Sec. 5, we show the results with the right-handed neutrinos for several representative values of their mass M_{R} . In Sec. 6, we show the allowed region when we vary both M_{R} and the top-quark mass m_t . In Sec. 7, we summarize and discuss our results. In Appendix A, we show the renormalization group equations (RGEs) that we employ in the computation of the effective potential. In Appendix B, we discuss that the shape of allowed region, shown in Secs. 4–6, can be understood in terms of the difference of potential shape.

2 Lower bound on tensor-to-scalar ratio

We present our basic strategy how to put a lower bound on r *without the knowledge of the physics at the higher Higgs-field value* $\varphi > \Lambda$, extending the analysis in Ref. [62]. In the slow-roll inflation, the observable A_s and r are written in terms of ϵ_V and V_{inf} :

$$A_s = \frac{1}{24\pi^2} \frac{1}{\epsilon_V} \frac{V_{\text{inf}}}{M_{\text{P}}^4}, \quad r = 16\epsilon_V, \quad (1)$$

where

$$\epsilon_V := \frac{M_{\text{P}}^2}{2} \left(\frac{V_{,\varphi}}{V} \right)^2, \quad (2)$$

is the slow-roll parameter. Eliminating ϵ_V , we obtain

$$r = \frac{2}{3\pi^2} \frac{1}{A_s} \frac{V_{\text{inf}}}{M_{\text{P}}^4}. \quad (3)$$

This gives a linear relation between r and V_{inf} since A_s is fixed by the CMB observation to be $A_s \simeq 2.2 \times 10^{-9}$ [79].

During the inflation, the inflaton field value is larger than Λ ; see Fig. 1. After the end of inflation, the field continues to roll down the potential hill and becomes the low-energy Higgs field that we know in the SM. In order not to prevent the rolling down to the EW scale, the maximum value of the effective potential in the region $\varphi \leq \Lambda$, which we call $V_{\varphi \leq \Lambda}^{\text{max}}$, must be smaller than the energy density during the inflation V_{inf} :

$$V_{\varphi \leq \Lambda}^{\text{max}} < V_{\text{inf}}. \quad (4)$$

We may rewrite Eq. (4), using Eq. (3), into the form:

$$r > \frac{2}{3\pi^2} \frac{1}{A_s} \frac{V_{\varphi \leq \Lambda}^{\text{max}}}{M_{\text{P}}^4}. \quad (5)$$

Thus, we obtain the lower bound on r from $V_{\varphi \leq \Lambda}^{\text{max}}$ only. For later convenience, we name the combination that appears in the right-hand side of Eq. (5) r_{bound} :

$$r_{\text{bound}} := \frac{2}{3\pi^2} \frac{1}{A_s} \frac{V_{\varphi \leq \Lambda}^{\text{max}}}{M_{\text{P}}^4}. \quad (6)$$

We emphasize that $V_{\varphi \leq \Lambda}^{\text{max}}$ is obtained from the physics at low-energy scales, while A_s and r in Eqs. (5) and (6), respectively, are the usual observable quantities that are defined at the horizon exit of the wavelength of the order of the CMB scale.

r_{bound} roughly scales as $\propto \Lambda^4$ so that one can rescale our results accordingly if needed. Our choice $\Lambda = 10^{17}$ GeV is motivated by the following facts:

- This value is (slightly below) the critical point at which both the Higgs quartic coupling and its beta function becomes zero; see e.g. Ref. [8].⁸
- This is the standard perturbative string scale; see any textbook of string theory or e.g. references from Ref. [63].

In the Higgs inflation, as we increase the Higgs field value, the potential starts to be modified from the SM one around the scale $\varphi \sim M_{\text{P}}/\sqrt{\xi}$ due to the change of the frames from Jordan to Einstein. Therefore we should take Λ to be this scale (or lower) so that $V|_{\varphi \leq \Lambda}$ is frame independent. In the non-critical Higgs inflation, the bound (5) becomes weak, while in the critical one, our analysis is valid; see footnote 6.

⁸If we instead used λ_{eff} , which is the Higgs effective potential divided by φ^4 [58], Λ would be $\Lambda \sim 10^{18}$ GeV, in which case the lower bound on r would become more stringent. We stay on the conservative side throughout this paper.

3 Z_2 Higgs-portal scalar model

In this paper, we employ the Higgs-portal Z_2 scalar dark matter. Below the scale Λ our Lagrangian is

$$\mathcal{L} = \mathcal{L}_{\text{SM}} + \frac{1}{2}(\partial_\mu S)^2 - \frac{1}{2}m_S^2 S^2 - \frac{\lambda_S}{4!}S^4 - \frac{\kappa}{2}S^2\Phi^\dagger\Phi, \quad (7)$$

where Φ is the SM Higgs doublet and S is the Higgs portal scalar field which has Z_2 symmetry. Hereafter we use $\varphi := \sqrt{2}\Phi^\dagger\Phi$. The singlet S is identified as the DM, whose mass is

$$m_{\text{DM}}^2 = m_S^2 + \frac{\kappa v^2}{2}, \quad (8)$$

where $v \simeq 246$ GeV is the Higgs vacuum expectation value (VEV). The parameters λ_S and κ affects $V_{\varphi \leq \Lambda}$ through the renormalization group (RG) running of the Higgs quartic coupling, while m_S does not. We assume that S does not acquire a Planck scale VEV and thus does not affect the inflation.

In this model, the thermal abundance of the DM fixes the relation between κ and m_{DM} in the non-resonant region [74]:⁹

$$\log_{10} \kappa \simeq -3.63 + 1.04 \log_{10} \frac{m_{\text{DM}}}{\text{GeV}}. \quad (9)$$

This relation allows us to convert m_{DM} into κ and vice versa. On the other hand, the spin-independent cross section and the dark-matter mass are related by [74]

$$\sigma_{\text{SI}} = \frac{\kappa^2 f_N^2}{4\pi} \left(\frac{m_n m_{\text{DM}}}{m_n + m_{\text{DM}}} \right)^2 \frac{m_n^2}{m_H^4 m_{\text{DM}}^2} \simeq 1.1 \times 10^{-45} \left(\frac{m_{\text{DM}}}{\text{TeV}} \right)^{0.08} \text{cm}^2. \quad (10)$$

The resultant 1.6σ constraint on the DM mass reads, as said in Introduction,

$$m_{\text{DM}} > 0.7 \pm 0.2 \text{ TeV}. \quad (11)$$

The uncertainty ± 0.2 TeV comes from that of the f_N ; see the caption of Fig. 2. Similarly, the 1.6σ results from the LUX [80] and XENON1T [81] experiments imply $m_{\text{DM}} > 0.5 \pm 0.1$ TeV and $m_{\text{DM}} > 0.6 \pm 0.1$ TeV, respectively. The corresponding lower bound on κ is $\kappa > 0.2$ for all the three experiments.

We will employ the pole mass of the top quark m_t as an input parameter for the RG analysis below. The Monte-Carlo mass of the top quark has been precisely measured to be $m_t^{\text{MC}} = 173.1 \pm 0.6$ GeV [82]. However, the relation between m_t^{MC} and the pole mass m_t is still unclear, and there remains uncertainty at least of 1 GeV; see e.g. Ref. [83] for a recent review. A theorist's combination of the pole mass, derived from the cross-section measurements, reads $m_t = 173.5 \pm 1.1$ GeV [82]. Hereafter we take conservatively two ranges:

$$171 \text{ GeV} < m_t < 176 \text{ GeV}, \quad (12)$$

$$169 \text{ GeV} < m_t < 178 \text{ GeV}, \quad (13)$$

which roughly corresponds to 2σ and 4σ ranges of the above combination, respectively.

⁹In the region of our interest, $0.1 \lesssim \kappa \lesssim 0.5$, this roughly translates as $m_{\text{DM}} \simeq \kappa \times 3.2$ TeV [75].

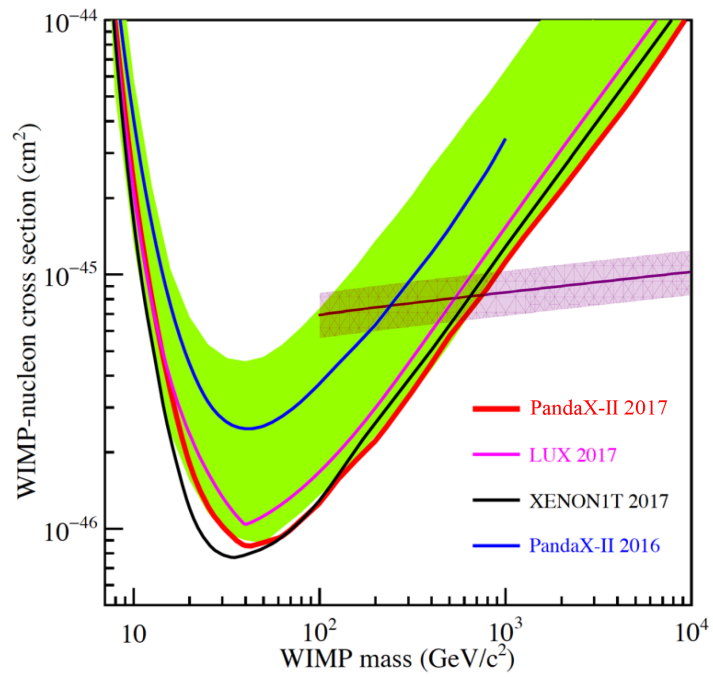


Figure 2: Fig. 5(a) in Ref. [76]. The upper side of each curve is excluded with 1.6σ C.L. We superimpose the purple line representing Eq. (10) and the light purple region denoting the error of σ_{SI} coming from the uncertainty of the overall coupling $f_N = 0.30 \pm 0.03$; see Ref. [74].

4 Analysis without heavy right-handed neutrinos

As shown in the previous section, we need to compute $V_{\varphi \leq \Lambda}$ in order to put the lower bound on r . We may find the excluded region in the r - m_{DM} plane by obtaining $V_{\varphi \leq \Lambda}^{\text{max}}$ as a function of κ for each fixed set of (λ_S, m_t) and converting κ to m_{DM} via Eq. (9). We first present our method of analysis in Sec. 4.1. Then we show our results in Sec. 4.2.

4.1 Method of analysis

We solve the RGEs for various (on-shell) values of λ_S and κ , as well as the pole mass of top quark m_t . First, we input the SM parameters at m_t that take into account the threshold corrections at the EW scale [10]. To take into account the threshold effect of the DM at the lowest order, we turn off λ and κ below m_{DM} given above.¹⁰ More details are explained in Appendix A. From the obtained running couplings, we determine $V_{\varphi \leq \Lambda}$. Then we exclude the parameter region in which V becomes negative in $\varphi \leq \Lambda$ or the perturbativity of couplings is violated. For the perturbativity, we demand that all the couplings are smaller than $\sqrt{4\pi} \simeq 3.5$ in all the region $\varphi \leq \Lambda$. This condition chooses the region $\kappa \leq 0.5$ ($m_{\text{DM}} \lesssim 1.6$ TeV) for $\lambda_S = 0$.¹¹ In this paper, we restrict to the case $\lambda_S = 0$ except for the right of Fig. 3 in which we instead take $\lambda_S = 0.6$ for comparison.¹²

4.2 Results

We plot the allowed region in r - m_{DM} plane for $\lambda_S = 0$ in the upper panel of Fig. 3. The region below each line is excluded, with its rainbow-color corresponding to each m_t value. In the lower panels, we show a region that is excluded regardless of the top-quark mass for $\lambda_S = 0$ (left) and for $\lambda_S = 0.6$ (right). The shape of the excluded region depends on how the Higgs potential changes as we vary the model parameters; see Appendix B for details. On both the panels, we also superimpose the constraints from the upper bound on r (blue band) and from the lower one on m_{DM} (red band).

Fig. 3 shows that the Planck constraint $r < 0.09$ [84] leads to bounds on m_t and m_{DM} :

$$171 \text{ GeV} < m_t < 175 \text{ GeV}, \quad (14)$$

$$m_{\text{DM}} \lesssim 1.1 \text{ TeV}. \quad (15)$$

This bound on m_{DM} is stricter than the above-mentioned perturbativity bound $m_{\text{DM}} \lesssim 1.6$ TeV.

When we take the lower bound by the PandaX-II experiment [76], $m_{\text{DM}} \gtrsim 0.7$ TeV ($\kappa \gtrsim 0.2$), we obtain the lower bound on tensor-to-scalar ratio

$$r \gtrsim 2 \times 10^{-3}. \quad (16)$$

We can explore this possibility in near-future experiments such as the POLARBEAR-2 [85], LiteBIRD [86] and CORE [87].

¹⁰As all the relevant couplings are small, higher order threshold corrections are at most few percent and are beyond the scope of our consideration.

¹¹See Fig. 1 in Ref. [75] for the allowed region in the λ_S - κ plane.

¹²We will see in the right of Fig. 3 that the large λ_S tends to narrower the allowed region. Therefore, it is more conservative to set $\lambda_S = 0$.

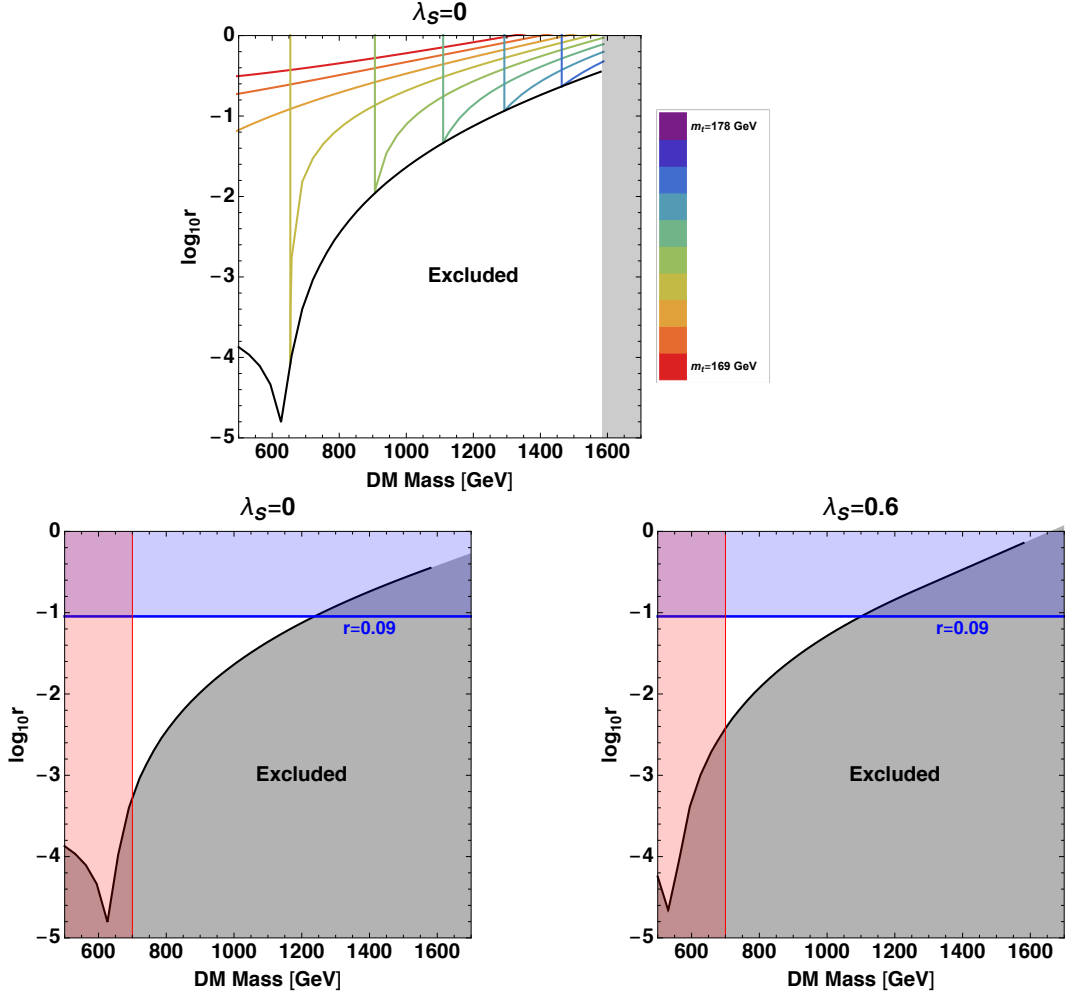


Figure 3: Upper: Allowed regions for $\lambda_S = 0$. For each m_t , the region above the line with corresponding color is allowed. Each vertical line denotes the lower bound on m_{DM} from the positivity of potential: $V_{\varphi \leq \Lambda} > 0$. The envelope of the rainbow-colored lines, indicated by the black line, gives the lower bound on r for each m_{DM} when one varies m_t . Lower: Excluded regions for $\lambda_S = 0$ (lower left) and $\lambda_S = 0.6$ (lower right). The blue and red regions are excluded by the upper bound on the tensor-to-scalar ratio $r < 0.09$ [84] and by lower bound on the DM mass $m_{\text{DM}} > 0.7$ TeV from PandaX-II [76], respectively.

	m_1 [eV]	m_2 [eV]	m_3 [eV]	Pattern
1. Normal Hierarchy	0 (set)	8.6×10^{-3}	5.1×10^{-2}	$m_1 \ll m_2 < m_3$
2. Inverted Hierarchy	5.0×10^{-2}	5.0×10^{-2}	0 (set)	$m_1 \simeq m_2 \gg m_3$
3. Degenerate (NO)	0.1 (set)	1.0×10^{-1}	1.1×10^{-1}	$m_1 \simeq m_2 \simeq m_3$
3. Degenerate (IO)	1.1×10^{-1}	1.1×10^{-1}	0.1 (set)	$m_1 \simeq m_2 \simeq m_3$

Table 1: Neutrino masses obtained from the absolute values of mass-squared differences in the notation of Ref. [88].

	Number of effective ν	Common mass m_ν [eV]
1. Normal Hierarchy	$n_\nu = 1$	5.1×10^{-2}
2. Inverted Hierarchy	$n_\nu = 2$	5.0×10^{-2}
3. Degenerate	$n_\nu = 3$	1.1×10^{-1}

Table 2: Common neutrino mass that we use as an input.

5 Analysis with right-handed neutrinos

We introduce the heavy right-handed neutrinos that account for the observed neutrino masses through the seesaw mechanism, and obtain the lower bound on r for each DM mass.

5.1 Method of analysis

The observational constraints on mass of left-handed neutrinos are the upper bound on the sum of masses and their squared differences; see e.g. Ref. [88]. Under this condition, we consider the following three typical patterns of mass relations:

1. Normal Hierarchy (NH, m_1 the lightest),
2. Inverted Hierarchy (IH, m_3 the lightest),
3. Degenerate (all masses comparable).

The mass pattern is most hierarchical when the lightest one is 0. In Degenerate case, the upper bound on the sum of neutrino masses reads $m_i \lesssim 0.1 \text{ eV}$.¹³ In Table 1, we show the

¹³The left-handed neutrino mass 0.1 eV for the three degenerate neutrinos corresponds to $\sum_i m_i = 0.3 \text{ eV}$. The 2σ upper bound from the TT-only analysis is $\sum_i m_i < 0.715 \text{ eV}$, while that from the TT+lensing+ext gives $\sum_i m_i < 0.234 \text{ eV}$ [84]. See also Refs. [89, 90] for more recent analyses that give a tighter bound $\sum_i m_i < 0.12 \text{ eV}$.

	m_t	M_R
$m_{\text{DM}} = 1 \text{ TeV}, r = 0.01$	$m_t < 174 \text{ GeV}$	$10^{14} \text{ GeV} \lesssim M_R \lesssim 10^{14.6} \text{ GeV}$
$m_{\text{DM}} = 1 \text{ TeV}, r = 0.001$	$173 \text{ GeV} < m_t < 174 \text{ GeV}$	$10^{14.1} \text{ GeV} \lesssim M_R \lesssim 10^{14.3} \text{ GeV}$
$m_{\text{DM}} = 1.5 \text{ TeV}, r = 0.01$	$170 \text{ GeV} < m_t < 178 \text{ GeV}$	$10^{14.6} \text{ GeV} \lesssim M_R \lesssim 10^{14.8} \text{ GeV}$
$m_{\text{DM}} = 1.5 \text{ TeV}, r = 0.001$	$m_t \simeq 177.8 \text{ GeV}$	$M_R \simeq 10^{14.6} \text{ GeV}$

Table 3: Constraints that will be obtained from future observations of m_{DM} and r for Normal Hierarchy.

mass pattern by setting the lightest one to be zero (0.1 eV) for the cases of normal/Inverted Hierarchy (Degenerate), using the mass-squared differences in Ref. [88]. For the three cases, we approximate the heaviest n_ν neutrinos as having a common mass m_ν and the remaining $3 - n_\nu$ ones as being massless as shown in Table 2.¹⁴

Under the existence of heavy right-handed neutrino, the remaining input parameters to determine $V_{\varphi \leq \Lambda}$ are λ_S , κ , m_t , and the right-handed neutrino mass $M_{R,i}$. For simplicity, we assume that $M_{R,i}$ ($i = 1, 2, 3$) are identical: $M_{R,i} = M_R$. The Yukawa coupling of neutrino is given by the seesaw mechanism: $y_\nu = \sqrt{2m_\nu M_R}/v$, with $v \simeq 246 \text{ GeV}$. The threshold effect is taken into account at the lowest order by turning on y_ν above M_R in the RGEs.¹⁵ See Appendix A for more details.

5.2 Results for Normal Hierarchy

We show the results for Normal Hierarchy, $n_\nu = 1$, in Fig. 4. The right-handed neutrino mass M_R is fixed in each panel: 10^{13} , 10^{14} , $10^{14.4}$ ($\simeq 2.5 \times 10^{14}$), $10^{14.5}$ ($\simeq 3.2 \times 10^{14}$), $10^{14.6}$ ($\simeq 4.0 \times 10^{14}$), and $10^{14.7}$ ($\simeq 5.0 \times 10^{14}$) in units of GeV. The color of envelope in each panel, denoted by the thick line, corresponds to the color in the plots in Sec. 6, in which the discussion for more general values of M_R will be given. Note that the thick line is obtained by tuning one parameter m_t for fixed M_R , and its minimum corresponds to the two parameter tuning of m_t and m_{DM} .

With the right-handed neutrino, we have one more theoretical parameter M_R in addition to m_t to determine from the observational constraints of r and m_{DM} . From Fig. 4, we see that the larger the M_R is, the smaller the allowed region becomes, for a given lower bound on m_t . This is because the right-handed neutrinos and the top quark have a similar effect on the Higgs potential, namely, they drives the Higgs quartic coupling smaller through the RG running towards high scales, and therefore they tend to make the Higgs potential negative if they both are heavy.¹⁶ If we e.g. set $m_t > 169 \text{ GeV}$, we have the constraint $M_R \lesssim 10^{14.8} \text{ GeV}$ ($\simeq 6.3 \times 10^{14} \text{ GeV}$); see also Fig. 8 in Sec. 6.

¹⁴If we want to consider a different m_ν , we may simply rescale the right-handed neutrino mass M_R in our results, since $m_\nu \propto M_R^{-1}$ by the seesaw mechanism.

¹⁵Higher order threshold corrections are beyond the scope of our consideration; see footnote 22.

¹⁶In this case, the vacuum stability is violated before the perturbativity.

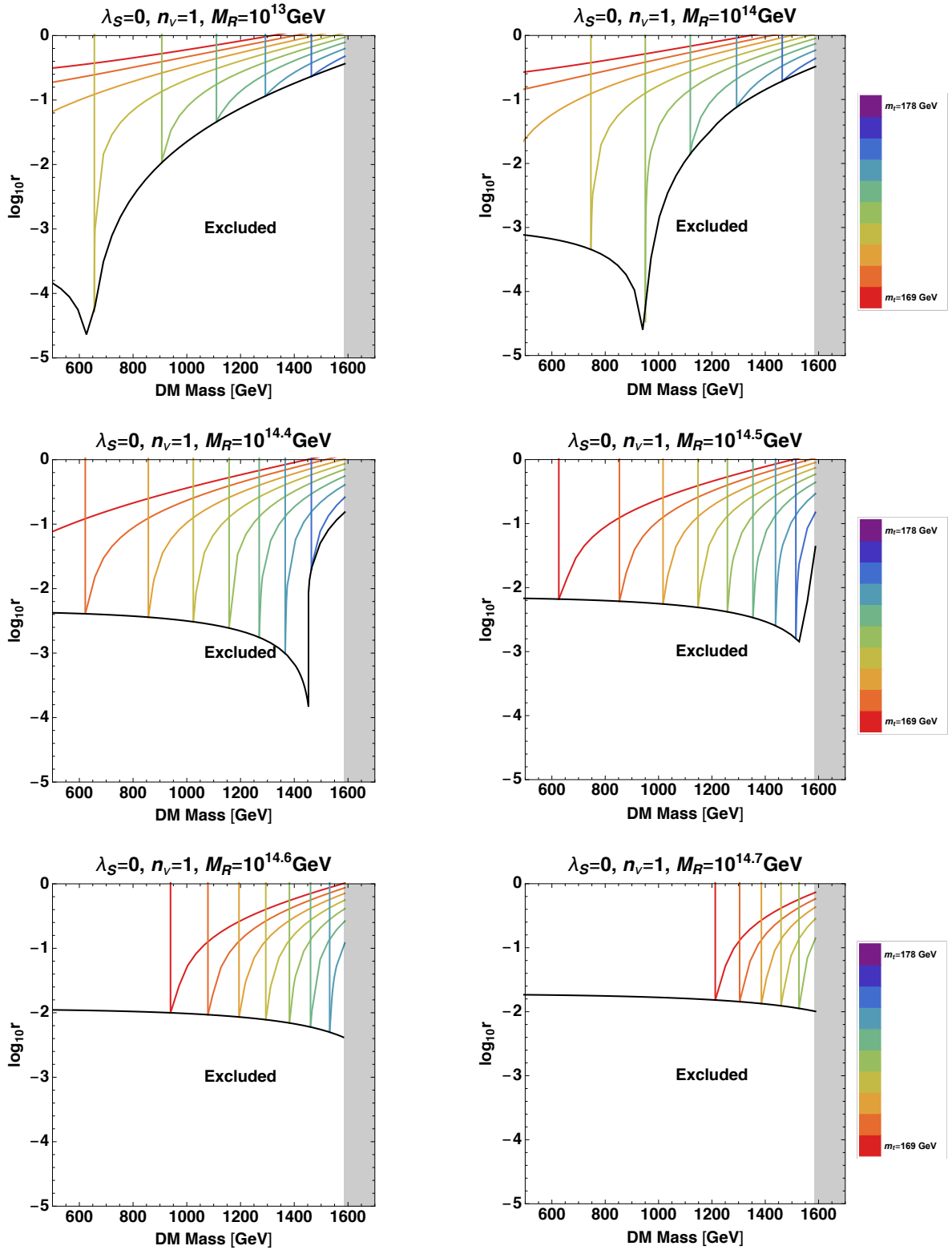


Figure 4: Allowed region for Normal Hierarchy with $\lambda_S = 0$. The right-handed neutrino mass M_R is increased in the order of the upper-left, upper-right, middle-left, . . . , lower-right panels. The bold line in each panel is the envelope of the m_t -fixed rainbow-colored lines, and gives the lower bound on r for the fixed M_R . See the caption of Fig. 3 for the shaded region.

As we increase M_R and switch panels in Fig. 4, we see that the value of m_{DM} at the minimum point of the envelope becomes larger: 600 GeV, 870 GeV, etc. In particular, it goes beyond the perturbativity bound, indicated by the gray band, when $M_R = 10^{14.7}$ GeV. Therefore, if the right-handed neutrino mass is larger than that, we have a stringent lower bound: $r \gtrsim 10^{-2}$. On the other hand, the plot with $M_R \lesssim 10^{13}$ GeV is almost the same as the case without right-handed neutrinos shown in the left of Fig. 3.

Let us see implications of future discoveries of the DM and r on the right-handed neutrino mass in the current context:¹⁷

- Suppose that $m_{\text{DM}} = 1$ TeV ($\kappa \simeq 0.31$) and $r = 0.01$ are found. Then the right-handed neutrino mass is predicted to be in the narrow range 10^{14} GeV $\lesssim M_R \lesssim 10^{14.6}$ GeV and the top-quark mass is constrained from above: $m_t < 174$ GeV.
- If we discover $m_{\text{DM}} = 1.5$ TeV ($\kappa \simeq 0.47$) and $r = 0.01$, we obtain the theoretical lower bound $M_R \gtrsim 10^{14.6}$ GeV, while the top quark mass is less constrained: 171 GeV $< m_t < 178$ GeV. However, M_R and m_t are highly correlated in this case. Therefore if one of them is fixed, the other is precisely predicted.
- See Table 3 for other pairs of m_{DM} and r . Generically the heavy DM mass tends to predict the heavy top-quark mass and M_R . The smaller the r is, the tighter the range of m_t . Especially, if we discover $m_{\text{DM}} = 1.5$ TeV and $r = 0.001$, m_t and M_R are accurately predicted.

We can predict r_{bound} or m_{DM} to some extent by considering typical input parameters. When we choose $m_t = 173$ GeV and $M_R = 10^{14}$ GeV, we obtain the bound $m_{\text{DM}} \sim 860$ GeV–970 GeV for $r < 0.09$.

5.3 Results for Inverted Hierarchy

We show the results for the case of Inverted Hierarchy ($n_\nu = 2$) in Fig. 5. In this case, the right-handed neutrinos lighter than $\sim 10^{13}$ GeV do not affect the analysis, similarly as in the case of Normal Hierarchy. However, the upper bound on M_R is slightly different: $M_R \lesssim 10^{14.7}$ GeV, see also Fig. 7. Let us summarize implications of future discoveries of the DM and r again on the right-handed neutrino mass in the current context:

- If we discover $m_{\text{DM}} = 1$ TeV and $r = 0.01$, we obtain $10^{13.9}$ GeV $\lesssim M_R \lesssim 10^{14.4}$ GeV and $m_t < 174$ GeV.
- If we discover $m_{\text{DM}} = 1.5$ TeV and $r = 0.01$, M_R must be larger than $\sim 10^{14.6}$ GeV and 170 GeV $< m_t < 178$ GeV. Although we cannot obtain the global narrow bounds on M_R and m_t , they are highly correlated as in the case of Normal Hierarchy.

See Table 4 for other pairs of m_{DM} and r .

¹⁷Here, we fit M_R and m_t from the future observation of m_{DM} and r . Instead, one might narrow down the error on the pole mass m_t e.g. at the High Luminosity LHC (HL-LHC) [91]. Then one may use m_t and m_{DM} as input parameters to predict M_R and r .

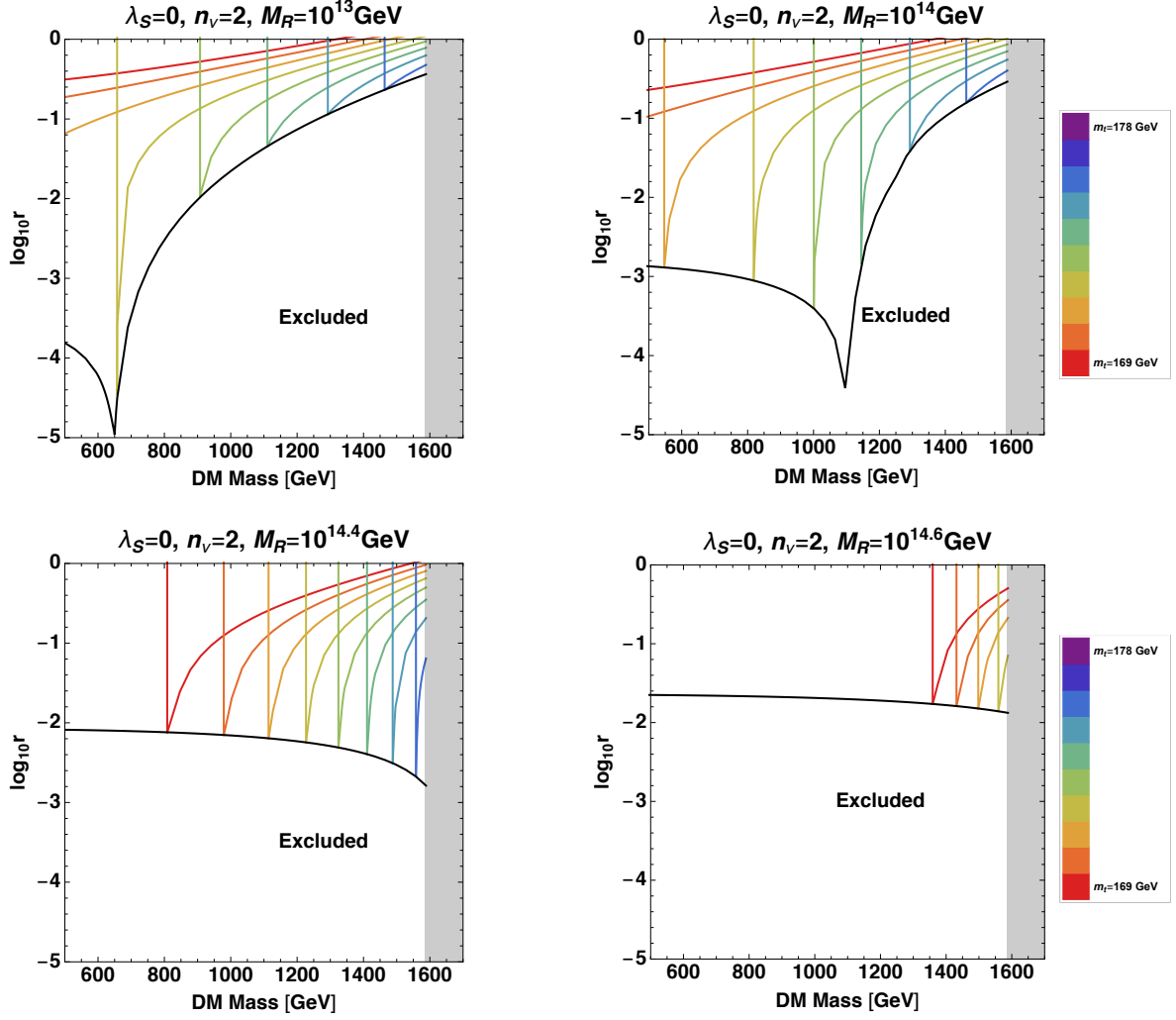


Figure 5: Allowed region for Inverted Hierarchy with $\lambda_S = 0$. See caption of Fig. 4 for the explanation.

	m_t	M_R
$m_{\text{DM}} = 1 \text{ TeV}, r = 0.01$	$m_t < 174 \text{ GeV}$	$10^{13.9} \text{ GeV} \lesssim M_R < 10^{14.5} \text{ GeV}$
$m_{\text{DM}} = 1 \text{ TeV}, r = 0.001$	$173 \text{ GeV} < m_t < 174 \text{ GeV}$	$10^{13.9} \text{ GeV} < M_R < 10^{14.2} \text{ GeV}$
$m_{\text{DM}} = 1.5 \text{ TeV}, r = 0.01$	$m_t < 178 \text{ GeV}$	$10^{14.4} \text{ GeV} < M_R \lesssim 10^{14.7} \text{ GeV}$
$m_{\text{DM}} = 1.5 \text{ TeV}, r = 0.001$	$177 \text{ GeV} < m_t < 178 \text{ GeV}$	$10^{14.4} \text{ GeV} < M_R < 10^{14.5} \text{ GeV}$

Table 4: Constraints obtained for Inverted Hierarchy.

5.4 Results for Degenerate case

We show the results for Degenerated case ($n_\nu = 3$) in Fig. 6. The right-handed neutrinos lighter than $\sim 10^{13}$ GeV do not affect the analysis, similarly as other cases. The upper bound on M_R is smaller than in other cases: $M_R \lesssim 10^{14.2}$ GeV $\simeq 1.6 \times 10^{14}$ GeV.

We summarize implications of future discoveries m_{DM} and r in Table 5. The right-handed neutrino mass tend to be lighter than hierarchical cases due to the heavy m_ν . However, the prediction of m_t is similar to the other cases.

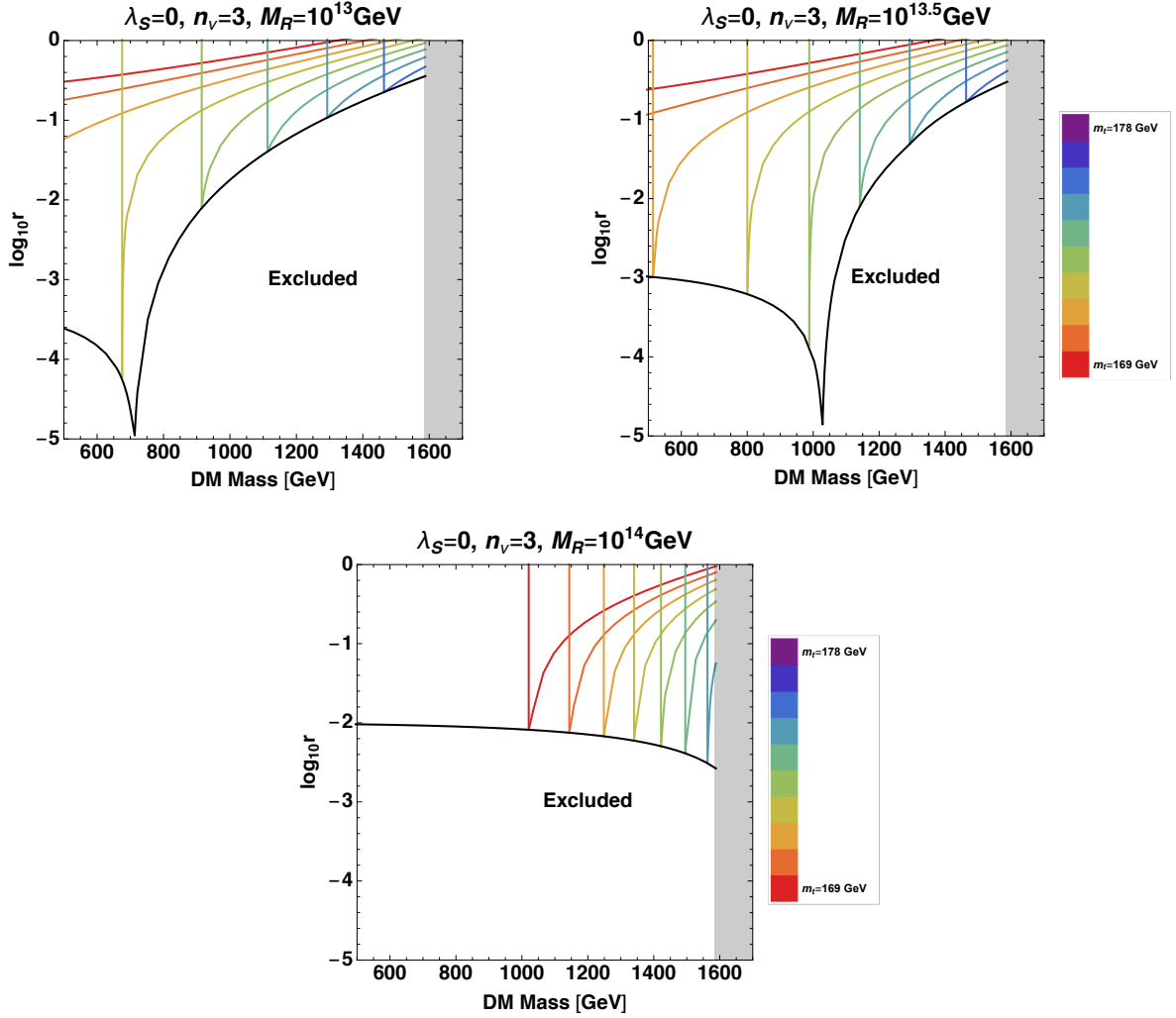


Figure 6: Allowed region for Degenerate case with $\lambda_S = 0$. See caption of Fig. 4 for the explanation.

	m_t	M_R
$m_{\text{DM}} = 1 \text{ TeV}, r = 0.01$	$m_t < 174 \text{ GeV}$	$10^{13.5} \text{ GeV} \lesssim M_R \lesssim 10^{14} \text{ GeV}$
$m_{\text{DM}} = 1 \text{ TeV}, r = 0.001$	$173 \text{ GeV} \lesssim m_t < 174 \text{ GeV}$	$10^{13.5} \text{ GeV} < M_R < 10^{13.8} \text{ GeV}$
$m_{\text{DM}} = 1.5 \text{ TeV}, r = 0.01$	$m_t < 178 \text{ GeV}$	$10^{14} \text{ GeV} \lesssim M_R \lesssim 10^{14.2} \text{ GeV}$
$m_{\text{DM}} = 1.5 \text{ TeV}, r = 0.001$	$176 \text{ GeV} < m_t < 178 \text{ GeV}$	$M_R \simeq 10^{14} \text{ GeV}$

Table 5: Constraints obtained for degenerate case.

6 Allowed region for all parameter space

In the previous section, we have plotted the bounds for various m_t in each panel of fixed M_R . In each panel, we have also shown the envelope of different m_t lines. This envelope is our theoretical lower bound on r for a given M_R .

In Sec. 6.1, we show these envelopes altogether in the same plot, and give the absolute lower bound on r for varying m_t and M_R . In Sec. 6.2, we see the same absolute lower bound in a different way, by changing the order of fixing m_t and M_R .

6.1 Lower bound on r for each M_R

In Figs. 7 and 8, we plot our theoretical lower bounds on r for various M_R when we allow the top-quark pole mass within roughly 2σ and 4σ ranges shown in Eqs. (12) and (13), respectively. We also give the envelope of these lines, which gives the allowed region for varying m_t and M_R . In the plot, each colored line represents the lower bound on r , and corresponds to the envelope denoted by the thick colored line in Secs. 5.2–5.4. We also show the absolute lower bound by the black line.¹⁸

We explain the envelope denoted by the black line in Fig. 7:

- We see that the allowed region is enlarged to

$$r \gtrsim 10^{-5} \quad (17)$$

from the $n_\nu = 0$ case in Eq. (16), which is read from the black line in Fig. 3 (being close the orange $M_R = 10^{13} \text{ GeV}$ line in Fig. 7). This is because the loop corrections of heavy right-handed neutrinos reduce $V_{\varphi \leq \Lambda}^{\text{max}}$.

¹⁸We have plotted the envelope, denoted by the black line, as follows: 1) Each M_R -fixed line has a minimum. Make an interpolating function which linearly join all these minimum points. 2) Each m_t -fixed line has a minimum. Make another interpolating function which linearly join all these minimum points. 3) Make a function that chooses the smaller value of these two for each m_{DM} . 4) In large m_{DM} region, we replace the interpolated bound with the lower bound determined by the maximal m_t ; see the caption of Fig. 9 to see how m_t gives the bound. Note that these interpolating functions are evaluated only for $600 \text{ GeV} < m_{\text{DM}} < 1600 \text{ GeV}$, and hence they are untrustworthy in the extrapolated regions $m_{\text{DM}} < 600 \text{ GeV}$ and $m_{\text{DM}} > 1600 \text{ GeV}$. This does not do any harm because these regions are already excluded by the direct DM search and by the perturbativity, respectively.

- The lower bound on r increases rapidly in the region $m_{\text{DM}} \gtrsim 1.3 \text{ TeV}$ due to the upper end of the parameter $m_t < 176 \text{ GeV}$.
- In the region near the envelope denoted by the black line, the two input parameters m_t and M_{R} are simultaneously tuned to minimize the potential height $V_{\varphi \leq \Lambda}^{\text{max}}$.
- If one allows to adjust the three parameters, m_t , M_{R} , and m_{DM} simultaneously, then the lowest point of the black line, $r \sim 10^{-5}$, is realized. This might be the case if some logic that demands the fine tuning, such as the multiple-point principle [21, 22, 23], is indeed applicable.

In Fig. 8, we plot for a wider range of the top-quark mass (13). The lower bound on r , denoted by the black line, increases in the region $m_{\text{DM}} \gtrsim 1.3 \text{ TeV}$ in the cases of $n_\nu = 1$ and 2 because of the difference of potential shapes explained in Appendix B, while its rise in the region $m_{\text{DM}} \gtrsim 1.5 \text{ TeV}$ is due to the upper end of the parameter $m_t < 178 \text{ GeV}$.

6.2 Lower bound on r for each m_t

In Fig. 9, we show the lower bound on r for each fixed m_t with M_{R} being varied. The envelope, denoted by the black line, is the same as the global lower bound on r in Sec. 6.1 except for the range explained in the caption.

The lowest possible value of m_{DM} for each m_t does not depend on the number of neutrinos n_ν . Therefore, for any given lower bound on m_t , we obtain the corresponding lower bound of m_{DM} without any assumptions on the other parameters in the neutrino sector. We see that the lowest point for a given m_t moves right as we increase m_t . This leads to a strong correlation between m_t and m_{DM} regardless of n_ν if $r < 10^{-3}$.

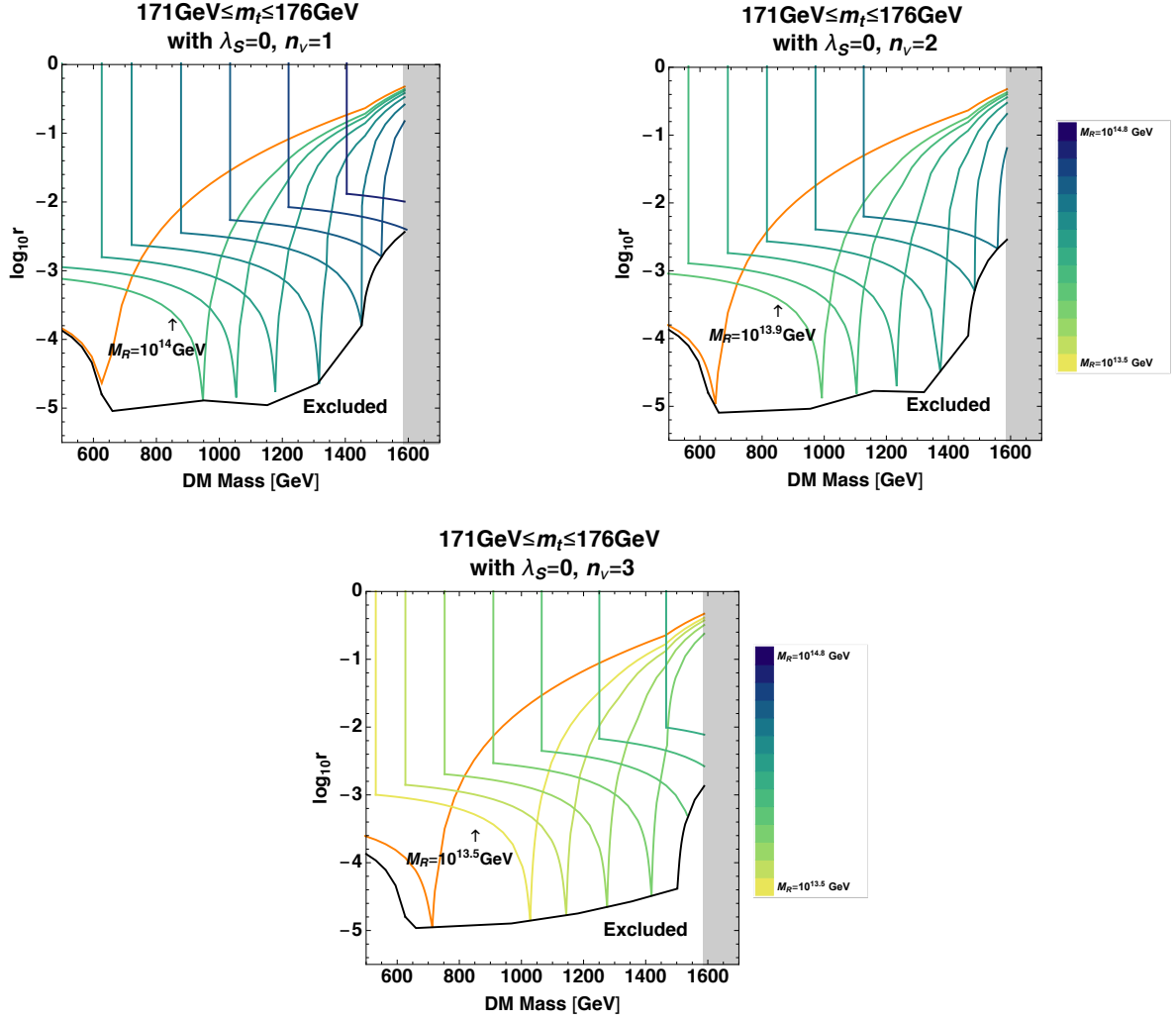


Figure 7: The lower bound on r for each fixed M_R (colored) and the envelope (black) with $\lambda_S = 0$ and $171 \text{ GeV} < m_t < 176 \text{ GeV}$. The orange line is for $M_R = 10^{13} \text{ GeV}$. The vertical colored line comes from the lower end, $m_t > 171 \text{ GeV}$. See the caption of Fig. 3 for the shaded region.

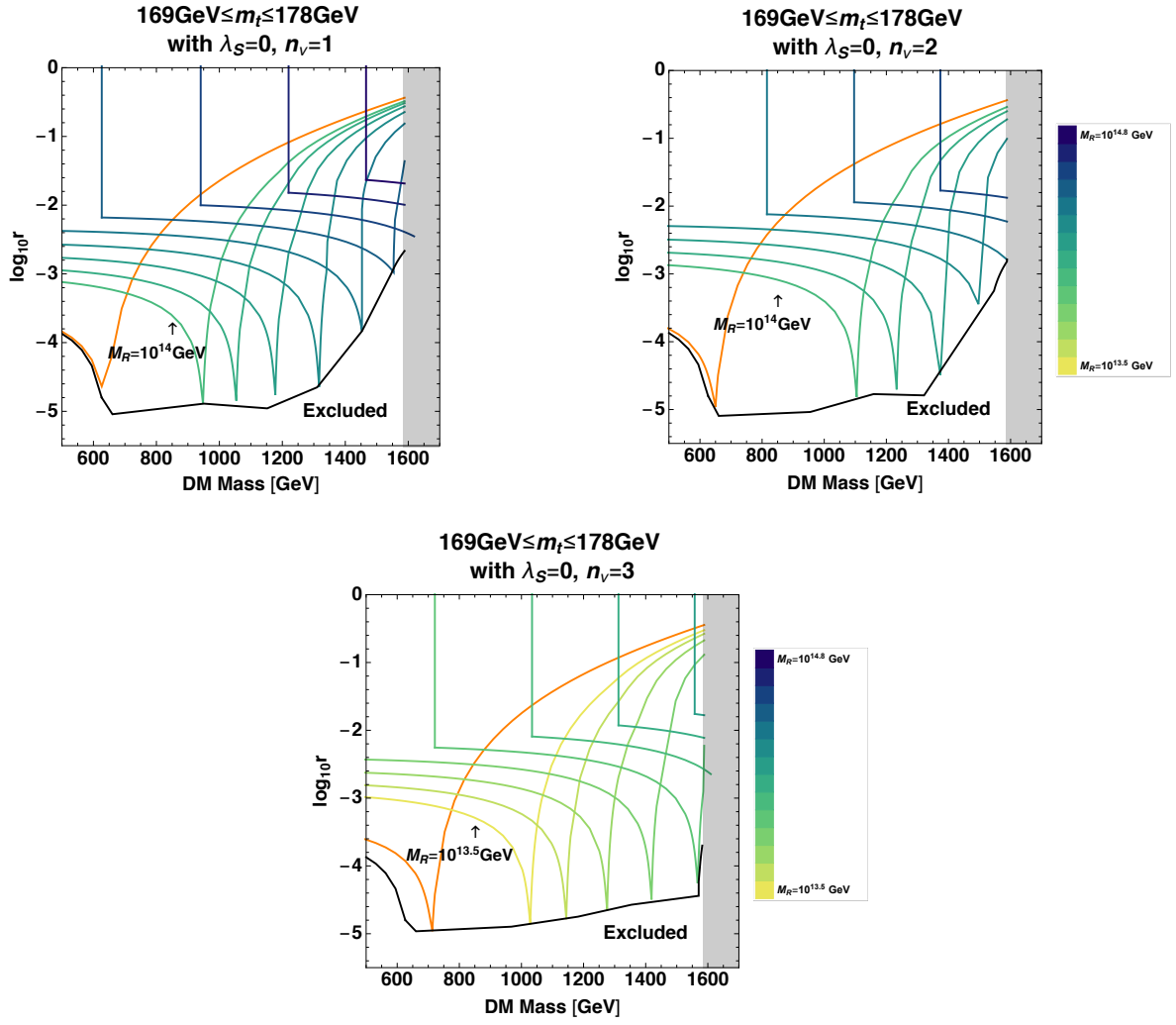


Figure 8: The same plot as in Fig. 7 for $169\text{ GeV} < m_t < 178\text{ GeV}$.

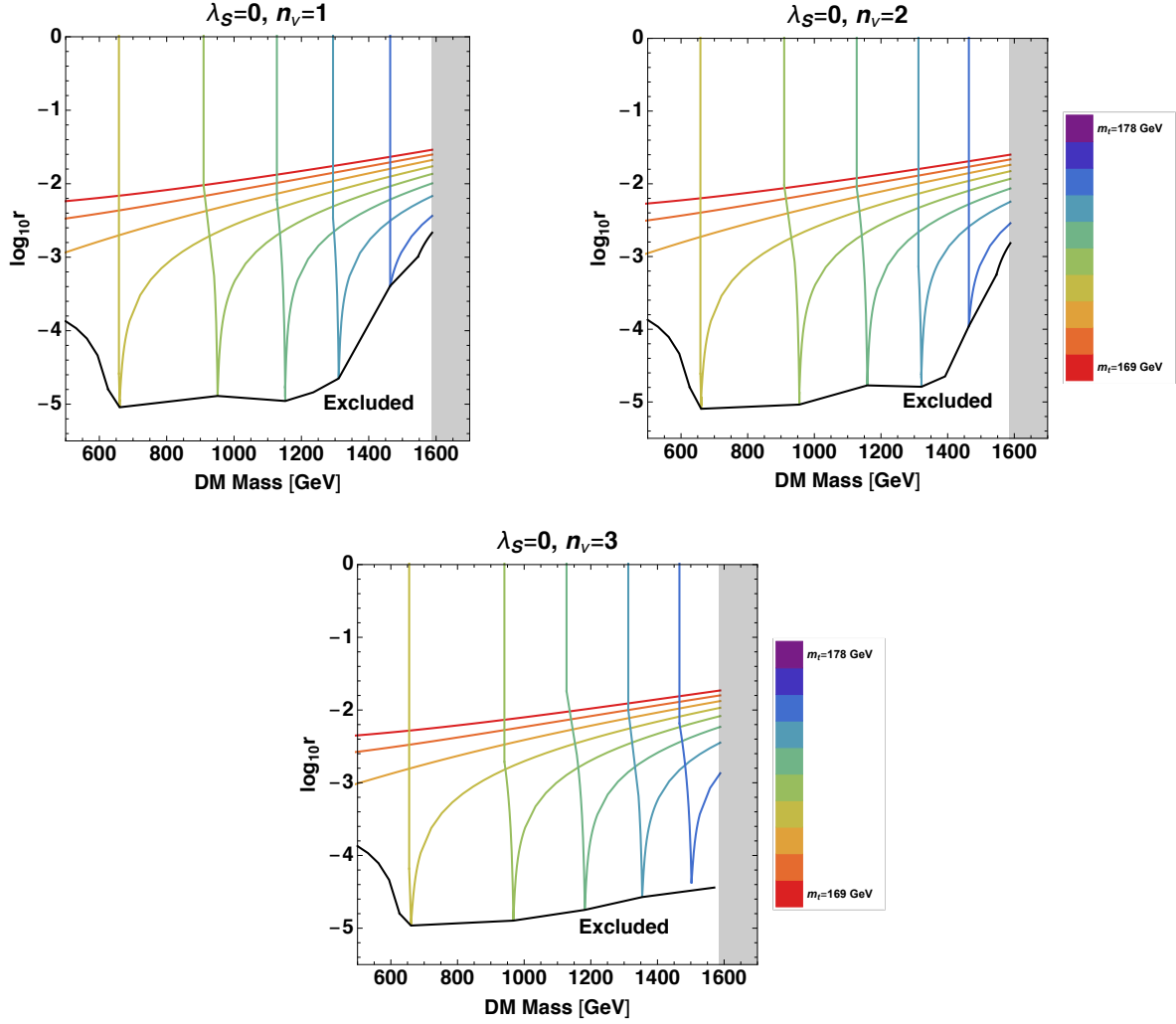


Figure 9: The lower bound on r for each fixed m_t (colored) with $\lambda_S = 0$. The black line is their envelope, which is identical to the ones in Figs. 7 and 8 except for their right-most boundary where they follow the $m_t = 176$ GeV (blue) and 178 GeV (purple) lines in this figure, respectively. See the left of Fig. 3 for the corresponding plot without right-handed neutrinos and for the explanation of the shaded region.

7 Summary and discussion

We have calculated the lower bound on the tensor-to-scalar ratio, r , for each given mass of the Higgs-portal Z_2 scalar dark matter, m_{DM} , under the simple assumption that the extrapolation of the Higgs-field direction plays the role of inflaton at $\varphi > \Lambda$. The advantage of our approach is that we may obtain the lower bound on r without knowing any detail of the high-scale physics.

In the case without the heavy right-handed neutrinos, we have obtained the theoretical bounds on (i) the DM mass $m_{\text{DM}} \lesssim 1.1 \text{ TeV}$, (ii) the tensor-to-scalar ratio $r \gtrsim 2 \times 10^{-3}$, and (iii) the pole mass of the top quark $171 \text{ GeV} < m_t < 175 \text{ GeV}$ from the current observational constraints $r < 0.09$ and $m_{\text{DM}} \gtrsim 0.7 \text{ TeV}$. We see that (i) and (ii) are rather stringent and are well within the near-future detection.

With the heavy right-handed neutrinos, we obtain the wider allowed region in the r - m_{DM} plane, $r \gtrsim 10^{-5}$ and $m_{\text{DM}} \lesssim 1.6 \text{ TeV}$, if we allow a three-parameter tuning. Although the region $r \lesssim 10^{-3}$ is hard for the planned near-future observations, we may still explore it in combination with the HL-LHC and future neutrino experiments because of the strong correlations between m_t , m_{DM} and the right-handed neutrino mass M_{R} .

The lower bound on r may slightly be affected when we relax the positivity condition on the Higgs potential by e.g. taking into account the thermal correction or by replacing it with the vacuum meta-stability. Because our bound is coming from the maximum value of effective Higgs potential, rather than the minimum, the lower bound on r would be reduced only by a factor of few even if we allow the negative value of the potential minimum of the order of the height of the potential maximum. Of course we should make sure that finally the EW vacuum is chosen in the late time in such a case.

In our RG analysis, we have assumed that all the fields are massless.¹⁹ In general, the non-minimal couplings $\xi\varphi^2 R$ and $\xi_S S^2 R$ cause the mass terms of the order of $\xi H^2 \varphi^2$ and $\xi_S H^2 S^2$, respectively. Under a classical field value φ_{cl} , we get

$$\xi H^2 \varphi^2 \sim \xi \lambda \frac{\varphi_{\text{cl}}^4}{M_{\text{P}}^2} \varphi^2, \quad \xi_S H^2 S^2 \sim \xi_S \lambda \frac{\varphi_{\text{cl}}^4}{M_{\text{P}}^2} S^2. \quad (18)$$

Such effective masses $\sqrt{\xi\lambda}\varphi_{\text{cl}}^2/M_{\text{P}}$ and $\sqrt{\xi_S\lambda}\varphi_{\text{cl}}^2/M_{\text{P}}$ are smaller enough than $\mu \sim \varphi_{\text{cl}}$ since we consider the non-minimal couplings $\xi, \xi_S \lesssim 10^2$ and the small quartic coupling $\lambda \ll 10^{-1}$ in the region $\varphi_{\text{cl}} \lesssim 10^{17} \text{ GeV}$.

It would be interesting to investigate the cosmology of our scenario after the inflation. For example, the Higgs field may be trapped at a false vacuum, and a mini inflation may results from it, depending on the initial condition at the end of the main inflation.²⁰ Afterwards, the true-vacuum bubbles should be created by the tunneling process, and the first order phase transition be completed by the bubble collision, which generates primordial gravitational waves and black holes. In addition, if the Higgs potential has an inflection point, the scalar perturbations could be enhanced, depending on how the slow-roll condition is well satisfied there, and could lead to another mechanism of the formation of primordial black holes. We hope to return to these issues in the future.

¹⁹The right-handed neutrinos are regarded massless at $\mu \sim \varphi_{\text{cl}} \gtrsim M_{\text{R}}$.

²⁰In this case, the dynamics of the Higgs field becomes chaotic in the sense that it is sensitive to the initial condition at the end of the main inflation.

	Value	Reference
Planck mass M_P	2.4353×10^{18} GeV	[82]
Higgs mass	125.09 GeV	[82]
Z bozon mass M_Z	91.1876 GeV	[82]
$\alpha_3(M_Z)$	0.1184	[10]
The expectation value of the Higgs field v	246 GeV	[82]

Table 6: Boundary condition for the RGEs.

Note added: After submission of the manuscript, there appeared newer bound [92], which roughly raise the lower bound on the dark matter mass up to $m_{\text{DM}} > 0.9 \pm 0.2$ TeV from Eq. (11).

Acknowledgement

We thank Tomohiro Abe, Xiangdong Ji, Kiyoharu Kawana, Jinsu Kim, Tae Geun Kim, Seong Chan Park, Stanislav Rusak, and Minoru Tanaka for useful comments. The work of Y.H., H.K., and K.O. are supported in part by JSPS KAKENHI Grant Nos. 16J06151 (YH), 16K05322 (HK), and 15K05053 (KO), respectively.

A Renormalization group equations

We have calculated the lower bound on r as follows:

1. Solve the RGEs (22)–(29) (shown in the end of this section) for given parameters. The effects from right-handed neutrino is introduced only at high energy scale $\varphi \geq M_R$: We set $n_\nu = 0$ and $M_R = 0$ in $\varphi < M_R$. As the boundary condition to solve the RGEs, we have used Eqs. (2.11)–(2.15) in [75] and the values in Table 6.²¹
2. Calculate the one-loop effective Higgs potential

$$V_{\varphi \leq \Lambda} = \frac{\lambda_{\text{eff}}}{4} \varphi^4 \quad (19)$$

where

$$\lambda_{\text{eff}} := e^{4\Gamma} \left[\lambda + \frac{1}{16\pi^2} \left\{ -3y_t^4 \left(\ln \frac{y_t^2}{2} - \frac{3}{2} + 2\Gamma \right) + \frac{3g_2^2}{8} \left(\ln \frac{g_2^2}{4} - \frac{5}{6} + 2\Gamma \right) \right. \right. \\ \left. \left. + \frac{3(g_Y^2 + g_2^2)^2}{16} \left(\ln \frac{g_Y^2 + g_2^2}{4} - \frac{5}{6} + 2\Gamma \right) - n_\nu y_\nu^4 \ln \left(\frac{M_R + \sqrt{M_R^2 + 4y_\nu^2 \varphi^2}}{2\sqrt{M_R^2 + \varphi^2}} \right) \right\} \right] \quad (20)$$

²¹This is based on Ref. [10], where the top Yukawa coupling and the electroweak gauge couplings are extracted with full 2-loop NNLO precision.

is the effective Higgs-self coupling.²² We set $\mu = \varphi$ when we calculate λ_{eff} ; see [58, 93] for the details about the renormalization scale μ of λ_{eff} . The one-loop wave-function renormalization

$$\Gamma(\varphi) = \int_{m_t}^{\varphi} \frac{1}{16\pi^2} \left(\frac{9}{4}g_2^2 + \frac{3}{4}g_Y^2 - 3y_t^2 - n_\nu y_\nu^2 \right) d \ln \mu \quad (21)$$

is taken into account.

3. Change the parameters using the false position method until the value of the potential minimum becomes sufficiently close to zero.
4. Calculate the maximum value of potential and obtain r_{bound} via Eq. (5).

We have obtained the RGEs for arbitrary n_ν combining the $n_\nu = 1$ RGEs [94] and the $n_\nu = 3$ ones [95]:

$$\frac{dg_Y}{d \ln \mu} = \frac{1}{16\pi^2} \frac{41}{6} g_Y^3 + \frac{g_Y^3}{(16\pi^2)^2} \left(\frac{199}{18} g_Y^2 + \frac{9}{2} g_2^2 + \frac{44}{3} g_3^2 - \frac{17}{6} y_t^2 - \frac{n_\nu}{2} y_\nu^2 \right), \quad (22)$$

$$\frac{dg_2}{d \ln \mu} = -\frac{1}{16\pi^2} \frac{19}{6} g_2^3 + \frac{g_2^3}{(16\pi^2)^2} \left(\frac{3}{2} g_Y^2 + \frac{35}{6} g_2^2 + 12g_3^2 - \frac{3}{2} y_t^2 - \frac{n_\nu}{2} y_\nu^2 \right), \quad (23)$$

$$\frac{dg_3}{d \ln \mu} = -\frac{7}{16\pi^2} g_3^3 + \frac{g_3^3}{(16\pi^2)^2} \left(\frac{11}{6} g_Y^2 + \frac{9}{2} g_2^2 - 26g_3^2 - 2y_t^2 \right), \quad (24)$$

$$\begin{aligned} \frac{dy_t}{d \ln \mu} = & \frac{y_t}{16\pi^2} \left(\frac{9}{2} y_t^2 + n_\nu y_\nu^2 - \frac{17}{12} g_Y^2 - \frac{9}{4} g_2^2 - 8g_3^2 \right) + \frac{y_t}{(16\pi^2)^2} \left\{ -12y_t^2 - \frac{9n_\nu}{4} y_\nu^4 - \frac{9n_\nu}{4} y_t^2 y_\nu^2 \right. \\ & + 6\lambda^2 + \frac{1}{4} \kappa^2 - 12\lambda y_t^2 + g_Y^2 \left(\frac{131}{16} y_t^2 + \frac{5n_\nu}{8} y_\nu^2 \right) + g_2^2 \left(\frac{225}{16} y_t^2 + \frac{5n_\nu}{8} y_\nu^2 \right) + 36g_3^2 y_t^2 \\ & \left. + \frac{1187}{216} g_Y^4 - \frac{23}{4} g_2^4 - 108g_3^4 - \frac{3}{4} g_Y^2 g_2^2 + 9g_2^2 g_3^2 + \frac{19}{9} g_3^2 g_Y^2 \right\}, \quad (25) \end{aligned}$$

$$\begin{aligned} \frac{d\lambda}{d \ln \mu} = & \frac{1}{16\pi^2} \left(\frac{1}{2} \kappa^2 + 24\lambda^2 - 3g_Y^2 \lambda - 9g_2^2 \lambda + 4n_\nu \lambda y_\nu^2 + \frac{3}{8} g_Y^4 + \frac{3}{4} g_Y^2 g_2^2 + \frac{9}{8} g_2^4 + 12\lambda y_t^2 - 6y_t^4 - 2n_\nu y_\nu^4 \right) \\ & + \frac{1}{(16\pi^2)^2} \left\{ -2\kappa^3 - 5\kappa^2 \lambda - 312\lambda^3 + 36\lambda^2 (g_Y^2 + 3g_2^2) - \lambda \left(\frac{629}{24} g_Y^4 - \frac{39}{4} g_Y^2 g_2^2 + \frac{73}{8} g_2^4 \right) \right. \\ & + \frac{305}{16} g_2^6 - \frac{289}{48} g_Y^2 g_2^4 - \frac{559}{48} g_Y^4 g_2^2 - \frac{379}{48} g_Y^6 - 32g_3^2 y_t^4 - \frac{8}{3} g_Y^2 y_t^4 - \frac{9}{4} g_2^4 y_t^2 - \frac{3n_\nu}{4} g_2^4 y_\nu^2 \\ & + \lambda y_t^2 \left(\frac{85}{6} g_Y^2 + \frac{45}{2} g_2^2 + 80g_3^2 \right) + \lambda y_\nu^2 \left(\frac{5n_\nu}{2} g_Y^2 + \frac{15n_\nu}{2} g_2^2 \right) + g_Y^2 y_t^2 \left(-\frac{19}{4} g_Y^2 + \frac{21}{2} g_2^2 \right) \\ & \left. - g_Y^2 y_\nu^2 \left(\frac{n_\nu}{4} g_Y^2 + \frac{n_\nu}{2} g_2^2 \right) - 144\lambda^2 y_t^2 - 48n_\nu y_\nu^2 - 3\lambda y_t^4 - n_\nu \lambda y_\nu^4 + 30y_t^6 + 10n_\nu y_\nu^6 \right\}, \quad (26) \end{aligned}$$

²² The last term in the braces is introduced to *naively* take into account the effect of the neutrino loop on the effective potential. We have checked that its effect is at most few percent.

$$\begin{aligned} \frac{dy_\nu}{d \ln \mu} &= \frac{y_\nu}{16\pi^2} \left\{ \left(n_\nu + \frac{3}{2} \right) y_\nu^2 + 3y_t^2 - \frac{3}{4}g_Y^2 - \frac{9}{4}g_2^2 \right\} + \frac{y_\nu}{(16\pi^2)^2} \left\{ - \left(\frac{9n_\nu}{2} - \frac{3}{2} \right) y_\nu^4 - \frac{27}{4}y_t^4 \right. \\ &\quad - \frac{27}{4}y_t^2 y_\nu^2 + 6\lambda^2 + \frac{1}{4}\kappa^2 - 12\lambda y_\nu^2 + g_Y^2 \left(\left(\frac{5n_\nu}{8} + \frac{93}{16} \right) y_\nu^2 + \frac{85}{24}y_t^2 \right) \\ &\quad \left. + g_2^2 \left(\left(\frac{15n_\nu}{8} + \frac{135}{16} \right) y_\nu^2 + \frac{45}{8}y_t^2 \right) + 20g_3^2 y_t^2 + \frac{35}{24}g_Y^4 - \frac{23}{4}g_2^4 - \frac{9}{4}g_Y^2 g_2^2 \right\}, \end{aligned} \quad (27)$$

$$\begin{aligned} \frac{d\kappa}{d \ln \mu} &= \frac{\kappa}{16\pi^2} \left(12\lambda + \lambda_S + 4\kappa + 6y_t^2 + 2n_\nu y_\nu^2 - \frac{3}{2}g_Y^2 - \frac{9}{2}g_2^2 \right) + \frac{\kappa}{(16\pi^2)^2} \left\{ - \frac{21}{2}\kappa^2 \right. \\ &\quad - 72\kappa\lambda - 60\lambda^2 - 6\kappa\lambda_S - \frac{5}{6}\lambda_S^2 - y_t^2(12\kappa + 72\lambda) - 4n_\nu\kappa y_\nu^2 - 24n_\nu\lambda y_\nu^2 \\ &\quad - \frac{27}{2}y_t^4 - \frac{9n_\nu}{2}y_\nu^4 + g_Y^2(\kappa + 24\lambda) + g_2^2(3\kappa + 72\lambda) + y_t^2 \left(\frac{85}{12}g_Y^2 + \frac{45}{4}g_2^2 + 40g_3^2 \right) \\ &\quad \left. + y_\nu^2 \left(\frac{5n_\nu}{4}g_Y^2 + \frac{15n_\nu}{4}g_2^2 \right) + \frac{557}{48}g_Y^4 - \frac{145}{16}g_2^4 + \frac{15}{8}g_Y^2 g_2^2 \right\}, \end{aligned} \quad (28)$$

$$\begin{aligned} \frac{d\lambda_S}{d \ln \mu} &= \frac{1}{16\pi^2} (3\lambda_S^2 + 12\kappa^2) + \frac{1}{(16\pi^2)^2} \left\{ - \frac{17}{3}\lambda_S^3 \right. \\ &\quad \left. - 20\kappa^2\lambda_S - 48\kappa^3 - 72\kappa^2 y_t^2 - 24n_\nu\kappa^2 y_\nu^2 + 24\kappa^2 g_Y^2 + 72\kappa^2 g_2^2 \right\}. \end{aligned} \quad (29)$$

B Explaining the form of envelope by potential shape

In this section, we explain the shape of envelopes denoted by the black or colored-thick line in the figures.

Let us start with the case without heavy right-handed neutrino (the left of Fig. 3). At the minimum point of envelope, the maximum value of the Higgs potential becomes smallest. In Fig. 10, we show the shape of potential near this point. At this minimum point, the height at the local maximum (at $\varphi \simeq 5 \times 10^{16}$ GeV in the case of Fig. 10) becomes identical to the height at $\varphi = \Lambda$. If the local potential minimum (at $\varphi = 9 \times 10^{16}$ GeV in the case of Fig. 10) is moved left, then the height at $\varphi = \Lambda$ becomes larger, while moved right, the height at the local maximum becomes larger. The left of the minimum point of the envelope is governed by the local maximum of the potential, while the right by the value at $\varphi = \Lambda$.

Now we turn to the case with right-handed neutrinos. The envelope is denoted by the

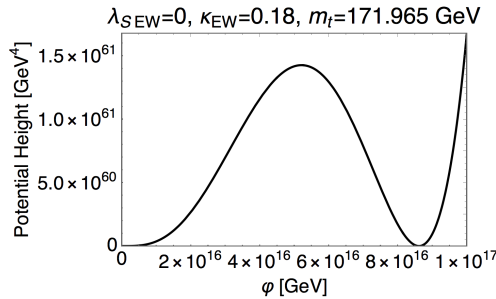


Figure 10: The shape of Higgs potential with the values of m_t and $m_{DM}(\kappa)$ that corresponds to a point near the minimum of the envelope in the left of Fig. 3.

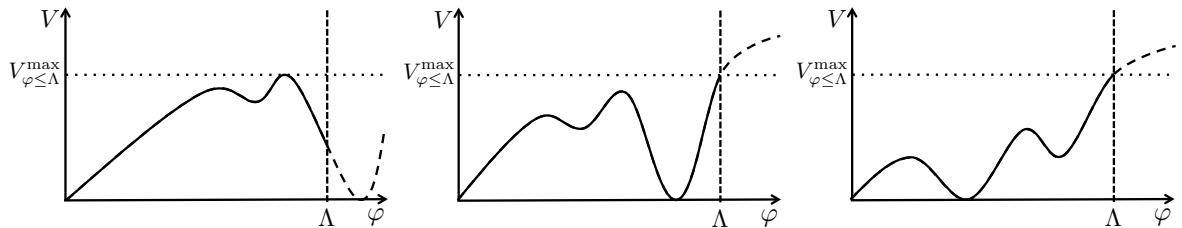


Figure 11: Left: Typical potential shape when its minimum is at $\varphi > \Lambda$. Center: Typical potential shape when the minimum at larger φ gives lower height. Right: Typical potential shape when the minimum at smaller φ gives lower height.

colored thick line in Figs. 4–6. We note that each envelope in Fig. 8 has, in addition to the cusp, one more (hardly seeable) non-smooth point, which is located, e.g. in the $n_\nu = 1$ panel, at $(m_{\text{DM}}, \log_{10} r) \sim (1050 \text{ GeV}, -1.5)$ for $M_{\text{R}} = 10^{14} \text{ GeV}$, $(1100 \text{ GeV}, -1.7)$ for $M_{\text{R}} = 10^{14.1} \text{ GeV}$, $(1150 \text{ GeV}, -2)$ for $M_{\text{R}} = 10^{14.2} \text{ GeV}$, and $(1220 \text{ GeV}, -2.6)$ for $M_{\text{R}} = 10^{14.3} \text{ GeV}$. This is because the Higgs potential has two local minima in general: The one at higher (lower) φ is due to the neutrino (top quark) contribution.²³ There are the following three kinds of potential shapes:

- (i) On the left side of the cusp of each envelope, the potential minimum at higher φ is located at $\varphi > \Lambda$; see the left of Fig. 11.
- (ii) In between the cusp and the non-smooth point of each envelope, there are two potential minima and the height of the one at larger φ is smaller; see the center of Fig. 11.
- (iii) On the right side of the non-smooth point of each envelope, there are two potential minima and the height of the one at lower φ is smaller; see the right of Fig. 11.

These two potential minima are degenerate on the black line in Figs. 7 and 8, and the cases (ii) and (iii) become identical.

References

- [1] V. Sanz and J. Setford, *Composite Higgs Models after Run 2*, *Adv. High Energy Phys.* **2018** (2018), 7168480, 1703.10190.
- [2] O. Witzel, *Review on Composite Higgs Models*, *PoS LATTICE2018* (2019), 006, 1901.08216.
- [3] M. Holthausen, K. S. Lim, and M. Lindner, *Planck scale Boundary Conditions and the Higgs Mass*, *JHEP* **1202** (2012), 037, 1112.2415.
- [4] F. Bezrukov, M. Y. Kalmykov, B. A. Kniehl, and M. Shaposhnikov, *Higgs Boson Mass and New Physics*, *JHEP* **1210** (2012), 140, 1205.2893.

²³Here we let the word “minimum” also stands for mere a concavity, namely, even when it is not really a minimum.

- [5] G. Degrandi, S. Di Vita, J. Elias-Miro, J. R. Espinosa, G. F. Giudice, G. Isidori, and A. Strumia, *Higgs mass and vacuum stability in the Standard Model at NNLO*, JHEP **08** (2012), 098, 1205.6497.
- [6] S. Alekhin, A. Djouadi, and S. Moch, *The top quark and Higgs boson masses and the stability of the electroweak vacuum*, Phys.Lett. **B716** (2012), 214–219, 1207.0980.
- [7] I. Masina, *The Higgs boson and Top quark masses as tests of Electroweak Vacuum Stability*, Phys.Rev. **D87** (2013), 053001, 1209.0393.
- [8] Y. Hamada, H. Kawai, and K.-y. Oda, *Bare Higgs mass at Planck scale*, Phys. Rev. **D87** (2013), no. 5, 053009, 1210.2538, [Erratum: Phys. Rev.D89,no.5,059901(2014)].
- [9] F. Jegerlehner, *The Standard model as a low-energy effective theory: what is triggering the Higgs mechanism?*, (2013), 1304.7813.
- [10] D. Buttazzo, G. Degrandi, P. P. Giardino, G. F. Giudice, F. Sala, A. Salvio, and A. Strumia, *Investigating the near-criticality of the Higgs boson*, JHEP **12** (2013), 089, 1307.3536.
- [11] V. Branchina and E. Messina, *Stability, Higgs Boson Mass and New Physics*, Phys.Rev.Lett. **111** (2013), 241801, 1307.5193.
- [12] A. Kobakhidze and A. Spencer-Smith, *The Higgs vacuum is unstable*, (2014), 1404.4709.
- [13] A. Spencer-Smith, *Higgs Vacuum Stability in a Mass-Dependent Renormalisation Scheme*, (2014), 1405.1975.
- [14] V. Branchina, E. Messina, and A. Platania, *Top mass determination, Higgs inflation, and vacuum stability*, (2014), 1407.4112.
- [15] V. Branchina, E. Messina, and M. Sher, *The lifetime of the electroweak vacuum and sensitivity to Planck scale physics*, (2014), 1408.5302.
- [16] A. V. Bednyakov, B. A. Kniehl, A. F. Pikelner, and O. L. Veretin, *Stability of the Electroweak Vacuum: Gauge Independence and Advanced Precision*, Phys. Rev. Lett. **115** (2015), no. 20, 201802, 1507.08833.
- [17] J. A. Casas, V. Di Clemente, A. Ibarra, and M. Quiros, *Massive neutrinos and the Higgs mass window*, Phys. Rev. **D62** (2000), 053005, hep-ph/9904295.
- [18] J. Elias-Miro, J. R. Espinosa, G. F. Giudice, G. Isidori, A. Riotto, and A. Strumia, *Higgs mass implications on the stability of the electroweak vacuum*, Phys. Lett. **B709** (2012), 222–228, 1112.3022.
- [19] C.-S. Chen and Y. Tang, *Vacuum stability, neutrinos, and dark matter*, JHEP **04** (2012), 019, 1202.5717.
- [20] W. Rodejohann and H. Zhang, *Impact of massive neutrinos on the Higgs self-coupling and electroweak vacuum stability*, JHEP **06** (2012), 022, 1203.3825.

- [21] C. D. Froggatt and H. B. Nielsen, *Standard model criticality prediction: Top mass 173 +/- 5-GeV and Higgs mass 135 +/- 9-GeV*, Phys. Lett. **B368** (1996), 96–102, hep-ph/9511371.
- [22] C. Froggatt, H. B. Nielsen, and Y. Takahashi, *Standard model Higgs boson mass from borderline metastability of the vacuum*, Phys.Rev. **D64** (2001), 113014, hep-ph/0104161.
- [23] H. B. Nielsen, *PREdicted the Higgs Mass*, (2012), 94–126, 1212.5716.
- [24] N. Haba, H. Ishida, N. Okada, and Y. Yamaguchi, *Multiple-point principle with a scalar singlet extension of the Standard Model*, PTEP **2017** (2017), no. 1, 013B03, 1608.00087.
- [25] N. Haba and T. Yamada, *Multiple-point principle realized with strong dynamics*, Phys. Rev. **D95** (2017), no. 11, 115015, 1703.04235.
- [26] K. A. Meissner and H. Nicolai, *Effective action, conformal anomaly and the issue of quadratic divergences*, Phys.Lett. **B660** (2008), 260–266, 0710.2840.
- [27] R. Foot, A. Kobakhidze, K. L. McDonald, and R. R. Volkas, *A Solution to the hierarchy problem from an almost decoupled hidden sector within a classically scale invariant theory*, Phys.Rev. **D77** (2008), 035006, 0709.2750.
- [28] S. Iso, N. Okada, and Y. Orikasa, *Classically conformal B – L extended Standard Model*, Phys.Lett. **B676** (2009), 81–87, 0902.4050.
- [29] S. Iso, N. Okada, and Y. Orikasa, *The minimal B – L model naturally realized at TeV scale*, Phys.Rev. **D80** (2009), 115007, 0909.0128.
- [30] T. Hur and P. Ko, *Scale invariant extension of the standard model with strongly interacting hidden sector*, Phys.Rev.Lett. **106** (2011), 141802, 1103.2571.
- [31] S. Iso and Y. Orikasa, *TeV Scale B-L model with a flat Higgs potential at the Planck scale - in view of the hierarchy problem -*, PTEP **2013** (2013), 023B08, 1210.2848.
- [32] M. Hashimoto, S. Iso, and Y. Orikasa, *Radiative symmetry breaking from flat potential in various U(1)' models*, Phys. Rev. **D89** (2014), no. 5, 056010, 1401.5944.
- [33] P. H. Chankowski, A. Lewandowski, K. A. Meissner, and H. Nicolai, *Softly broken conformal symmetry and the stability of the electroweak scale*, (2014), 1404.0548.
- [34] A. Kobakhidze and K. L. McDonald, *Comments on the Hierarchy Problem in Effective Theories*, (2014), 1404.5823.
- [35] A. Gorsky, A. Mironov, A. Morozov, and T. Tomaras, *Is the Standard Model saved asymptotically by conformal symmetry?*, Zh.Eksp.Teor.Fiz. **147** (2015), 399–409, 1409.0492.
- [36] J. Kubo, K. S. Lim, and M. Lindner, *Electroweak Symmetry Breaking via QCD*, Phys.Rev.Lett. **113** (2014), 091604, 1403.4262.
- [37] R. Foot, A. Kobakhidze, and A. Spencer-Smith, *Criticality in the scale invariant standard model (squared)*, (2014), 1409.4915.
- [38] K. Kawana, *Criticality and Inflation of the Gauged B-L Model*, (2015), 1501.04482.

- [39] A. Latosinski, A. Lewandowski, K. A. Meissner, and H. Nicolai, *Conformal Standard Model with an extended scalar sector*, JHEP **10** (2015), 170, 1507.01755.
- [40] N. Haba, H. Ishida, R. Takahashi, and Y. Yamaguchi, *Gauge coupling unification in a classically scale invariant model*, JHEP **02** (2016), 058, 1511.02107.
- [41] N. Haba, H. Ishida, N. Kitazawa, and Y. Yamaguchi, *A new dynamics of electroweak symmetry breaking with classically scale invariance*, Phys. Lett. **B755** (2016), 439–443, 1512.05061.
- [42] J. Kubo and M. Yamada, *Scale genesis and gravitational wave in a classically scale invariant extension of the standard model*, JCAP **1612** (2016), no. 12, 001, 1610.02241.
- [43] N. Haba and T. Yamada, *Strong dynamics in a classically scale invariant extension of the standard model with a flat potential*, Phys. Rev. **D95** (2017), no. 11, 115016, 1701.02146.
- [44] S. Iso, P. D. Serpico, and K. Shimada, *QCD-Electroweak First-Order Phase Transition in a Supercooled Universe*, Phys. Rev. Lett. **119** (2017), no. 14, 141301, 1704.04955.
- [45] A. Lewandowski, K. A. Meissner, and H. Nicolai, *Conformal Standard Model, Leptogenesis and Dark Matter*, (2017), 1710.06149.
- [46] M. Shaposhnikov and C. Wetterich, *Asymptotic safety of gravity and the Higgs boson mass*, Phys.Lett. **B683** (2010), 196–200, 0912.0208.
- [47] C. Wetterich and M. Yamada, *Gauge hierarchy problem in asymptotically safe gravity—the resurgence mechanism*, Phys. Lett. **B770** (2017), 268–271, 1612.03069.
- [48] A. Eichhorn, Y. Hamada, J. Lumma, and M. Yamada, *Quantum gravity fluctuations flatten the Planck-scale Higgs-potential*, (2017), 1712.00319.
- [49] Y. Kawamura, *Naturalness, Conformal Symmetry and Duality*, PTEP **2013** (2013), no. 11, 113B04, 1308.5069.
- [50] Y. Kawamura, *Gauge hierarchy problem, supersymmetry and fermionic symmetry*, (2013), 1311.2365.
- [51] H. Kawai and T. Okada, *Solving the Naturalness Problem by Baby Universes in the Lorentzian Multiverse*, Prog.Theor.Phys. **127** (2012), 689–721, 1110.2303.
- [52] H. Kawai, *Low energy effective action of quantum gravity and the naturalness problem*, Int.J.Mod.Phys. **A28** (2013), 1340001.
- [53] Y. Hamada, H. Kawai, and K. Kawana, *Evidence of the Big Fix*, Int.J.Mod.Phys. **A29** (2014), no. 17, 1450099, 1405.1310.
- [54] K. Kawana, *Reconsideration of the Coleman’s Baby Universe*, (2014), 1405.2743.
- [55] Y. Hamada, H. Kawai, and K. Kawana, *Weak Scale From the Maximum Entropy Principle*, PTEP **2015** (2014), no. 3, 033B06, 1409.6508.
- [56] Y. Hamada, H. Kawai, K.-y. Oda, and S. C. Park, *Higgs inflation still alive*, Phys.Rev.Lett. **112** (2014), 241301, 1403.5043.

- [57] Bezrukov, Fedor and Shaposhnikov, Mikhail, *Higgs inflation at the critical point*, (2014), 1403.6078.
- [58] Y. Hamada, H. Kawai, K.-y. Oda, and S. C. Park, *Higgs inflation from Standard Model criticality*, Phys. Rev. **D91** (2015), 053008, 1408.4864.
- [59] J. L. Cook, L. M. Krauss, A. J. Long, and S. Sabharwal, *Is Higgs inflation ruled out?*, Phys. Rev. **D89** (2014), no. 10, 103525, 1403.4971.
- [60] D. S. Salopek, J. R. Bond, and J. M. Bardeen, *Designing Density Fluctuation Spectra in Inflation*, Phys. Rev. **D40** (1989), 1753.
- [61] F. Bezrukov and M. Shaposhnikov, *The Standard Model Higgs boson as the inflaton*, Phys.Lett. **B659** (2008), 703–706, 0710.3755.
- [62] Y. Hamada, H. Kawai, and K.-y. Oda, *Minimal Higgs inflation*, PTEP **2014** (2014), 023B02, 1308.6651.
- [63] Y. Hamada, H. Kawai, and K.-y. Oda, *Eternal Higgs inflation and the cosmological constant problem*, Phys. Rev. **D92** (2015), 045009, 1501.04455.
- [64] V. Silveira and A. Zee, *SCALAR PHANTOMS*, Phys.Lett. **B161** (1985), 136.
- [65] J. McDonald, *Gauge singlet scalars as cold dark matter*, Phys.Rev. **D50** (1994), 3637–3649, hep-ph/0702143.
- [66] C. Burgess, M. Pospelov, and T. ter Veldhuis, *The Minimal model of nonbaryonic dark matter: A Singlet scalar*, Nucl.Phys. **B619** (2001), 709–728, hep-ph/0011335.
- [67] H. Davoudiasl, R. Kitano, T. Li, and H. Murayama, *The New minimal standard model*, Phys.Lett. **B609** (2005), 117–123, hep-ph/0405097.
- [68] B. Patt and F. Wilczek, *Higgs-field portal into hidden sectors*, (2006), hep-ph/0605188.
- [69] B. Grzadkowski and J. Wudka, *Pragmatic approach to the little hierarchy problem: the case for Dark Matter and neutrino physics*, Phys.Rev.Lett. **103** (2009), 091802, 0902.0628.
- [70] A. Drozd, B. Grzadkowski, and J. Wudka, *Multi-Scalar-Singlet Extension of the Standard Model - the Case for Dark Matter and an Invisible Higgs Boson*, JHEP **1204** (2012), 006, 1112.2582.
- [71] N. Haba, K. Kaneta, and R. Takahashi, *Planck scale boundary conditions in the standard model with singlet scalar dark matter*, JHEP **1404** (2014), 029, 1312.2089.
- [72] S. Baek, P. Ko, and W.-I. Park, *Invisible Higgs Decay Width vs. Dark Matter Direct Detection Cross Section in Higgs Portal Dark Matter Models*, Phys. Rev. **D90** (2014), no. 5, 055014, 1405.3530.
- [73] J. Kim, P. Ko, and W.-I. Park, *Higgs-portal assisted Higgs inflation with a sizeable tensor-to-scalar ratio*, JCAP **1702** (2017), no. 02, 003, 1405.1635.

- [74] J. M. Cline, K. Kainulainen, P. Scott, and C. Weniger, *Update on scalar singlet dark matter*, Phys. Rev. **D88** (2013), 055025, 1306.4710, [Erratum: Phys. Rev.D92,no.3,039906(2015)].
- [75] Y. Hamada, H. Kawai, and K.-y. Oda, *Predictions on mass of Higgs portal scalar dark matter from Higgs inflation and flat potential*, JHEP **07** (2014), 026, 1404.6141.
- [76] PandaX-II, X. Cui et al., *Dark Matter Results From 54-Ton-Day Exposure of PandaX-II Experiment*, Phys. Rev. Lett. **119** (2017), no. 18, 181302, 1708.06917.
- [77] P. Minkowski, $\mu \rightarrow e\gamma$ at a Rate of One Out of 10^9 Muon Decays?, Phys. Lett. **67B** (1977), 421–428.
- [78] T. Yanagida, in *Proceedings of the Workshop on Unified Theory and Baryon Number of the Universe*, edited by O. Sawada and A. Sugamoto (KEK, Tokyo, 1979), p. 95; M. Gell-Mann, P. Ramond, and R. Slanski, in *Supergravity*, edited by P. van Nieuwenhuizen and D. Freedman (North-Holland, Amsterdam, 1979) arXiv:1306.4669; S. L. Glashow, in *Proceedings of the Cargèse Summer Institute on Quarks and Leptons*, Cargèse, July 9–29, 1979, eds. M. Lévy et al. (Plenum, 1980, New York), p. 707; R. N. Mohapatra and G. Senjanovic, *Neutrino Mass and Spontaneous Parity Violation*, Phys. Rev. Lett. **44** (1980) 912.
- [79] Planck, P. A. R. Ade et al., *Planck 2015 results. XX. Constraints on inflation*, Astron. Astrophys. **594** (2016), A20, 1502.02114.
- [80] LUX, D. S. Akerib et al., *Results from a search for dark matter in the complete LUX exposure*, Phys. Rev. Lett. **118** (2017), no. 2, 021303, 1608.07648.
- [81] XENON, E. Aprile et al., *First Dark Matter Search Results from the XENON1T Experiment*, (2017), 1705.06655.
- [82] Particle Data Group, C. Patrignani et al., *Review of Particle Physics*, Chin. Phys. **C40** (2016), no. 10, 100001.
- [83] G. Cortiana, *Top-quark mass measurements: review and perspectives*, Rev. Phys. **1** (2016), 60–76, 1510.04483.
- [84] Planck, P. A. R. Ade et al., *Planck 2015 results. XIII. Cosmological parameters*, Astron. Astrophys. **594** (2016), A13, 1502.01589.
- [85] POLARBEAR, Y. Inoue et al., *POLARBEAR-2: an instrument for CMB polarization measurements*, Proc. SPIE Int. Soc. Opt. Eng. **9914** (2016), 99141I, 1608.03025.
- [86] T. Matsumura et al., *Mission design of LiteBIRD*, (2013), 1311.2847, [J. Low. Temp. Phys.176,733(2014)].
- [87] CORE, J. Delabrouille et al., *Exploring Cosmic Origins with CORE: Survey requirements and mission design*, (2017), 1706.04516.
- [88] F. Capozzi, E. Di Valentino, E. Lisi, A. Marrone, A. Melchiorri, and A. Palazzo, *Global constraints on absolute neutrino masses and their ordering*, (2017), 1703.04471.

- [89] E. Giusarma, M. Gerbino, O. Mena, S. Vagnozzi, S. Ho, and K. Freese, *Improvement of cosmological neutrino mass bounds*, Phys. Rev. **D94** (2016), no. 8, 083522, 1605.04320.
- [90] S. Vagnozzi, E. Giusarma, O. Mena, K. Freese, M. Gerbino, S. Ho, and M. Lattanzi, *Unveiling ν secrets with cosmological data: neutrino masses and mass hierarchy*, Phys. Rev. **D96** (2017), no. 12, 123503, 1701.08172.
- [91] CMS Collaboration, *Updates on Projections of Physics Reach with the Upgraded CMS Detector for High Luminosity LHC*, (2016), <https://cds.cern.ch/record/2221747>.
- [92] XENON, E. Aprile et al., *Dark Matter Search Results from a One Ton-Year Exposure of XENON1T*, Phys. Rev. Lett. **121** (2018), no. 11, 111302, 1805.12562.
- [93] Y. Hamada, H. Kawai, Y. Nakanishi, and K.-y. Oda, *Meaning of the field dependence of the renormalization scale in Higgs inflation*, Phys. Rev. **D95** (2017), no. 10, 103524, 1610.05885.
- [94] N. Haba, H. Ishida, and R. Takahashi, *Higgs inflation and Higgs portal dark matter with right-handed neutrinos*, PTEP **2015** (2015), no. 5, 053B01, 1405.5738.
- [95] K. Kawana, *Multiple Point Principle of the Standard Model with Scalar Singlet Dark Matter and Right Handed Neutrinos*, PTEP **2015** (2015), 023B04, 1411.2097.